Toward Modeling Thermoresponsive Polymer Networks: A Molecular Dynamics Simulation Study of *N*-Isopropyl Acrylamide Co-oligomers

Ester Chiessi,* Alice Lonardi, and Gaio Paradossi

Dipartimento di Scienze e Tecnologie Chimiche, University of Rome Tor Vergata, Via della Ricerca Scientifica I, 00133 Rome, Italy

Received: December 28, 2009; Revised Manuscript Received: April 30, 2010

Polymer microgels of poly(vinyl alcohol)/poly(methacrylate-*co*-*N*-isopropyl acrylamide) showed a thermoresponsive behavior, suitable for application in drug delivery (*Biomacromolecules* **2009**, *10*, 1589). In this work molecular dynamics (MD) methods were used to explain which structural aspects are determining for thermoresponsivity and how water properties in the hydrogel are influenced. Two topologically different models of the junction domain in the hydrogel at the experimental hydration degree were studied at 293 and 323 K, below and above the transition temperature. MD simulations of the corresponding oligomers of poly(*N*-isopropyl acrylamide) were also performed for a comparison. Simulation results provided an atomic detailed description of the temperature induced modifications in the microgel network and of water dynamics, in agreement with available experimental findings.

1. Introduction

In the last decades, a large research effort has been devoted to exploit the peculiar properties of soft matter in biomedical applications[1−4] and, in this context, several studies have been reported about the development of microgels based on biocompatible polymer matrixes for controlled drug delivery.[3,5,6] One of the most valuable requirements in these systems is the capability to modify properties such as hydration degree, internal texture, specific surface as a function of external stimuli, such as a change in temperature, pH, and ionic strength.[7] Polymer residues with ionizable groups can impart a sensitivity to pH and/or ionic strength,[8−10] whereas the sensitivity of the network to temperature in water is obtained with amphiphilic polymers, when the balance between hydrophilicity and hydrophobicity can be modulated by temperature. In the latter systems, the polymer−solvent interaction is thermodynamically favorable for temperatures lower than an intrinsic lower critical solution temperature (LCST), and under this value a relaxed solvated conformational state is preferred. When the temperature exceeds the LCST, the polymer−polymer interactions become preferable, and the chains collapse in a coiled state. This behavior is shown in aqueous environment by a few polymers, such as poly(oxyethylene) in dilute solution,[11,12] poly(vinyl methyl ether),[13] hydroxypropyl-cellulose,[14] and more complex macromolecular systems, such as pluronic triblock copolymers composed of poly(ethylene oxide)−poly(propylene oxide)−poly(ethylene oxide).[15] An example of LCST-type phase separation in non aqueous solvent is provided by poly(benzyl methacrylate) in hydrophobic ionic liquids.[16] However, among the thermosensitive polymers, the poly-*N*-isopropyl acrylamide (p(NIPAAm)) is undoubtedly the most studied.[17] The volume phase transition of linear p(NIPAAm) as a function of temperature, known since the 1960s,[18] is evidenced in aqueous solutions with an increase of the turbidity eventually followed by precipitation at around 307 K, the p(NIPAAm) LCST.[17] A large number of papers continues to be published in the scientific literature, both on the experimental characterization of the volume phase transition[19−25] and on the development of complex polymer systems based on p(NIPAAm) for several applications.[26−28]

In this outline, the leading idea to obtain an injectable polymer microdevice for a targeted and controlled drug release guided us to synthesize novel temperature-sensitive hydrogel microparticles of poly(vinyl alcohol)/poly(methacrylate-*co*-*N*-isopropyl acrylamide) (PVA-MA-NIPAAm).[6] In PVA-MA-NIPAAm microgels, the polymer scaffold forms a chemically cross-linked network with a residue composition PVA:MA:NIPAAm of 20:1:2.5 and 20:1:4, depending on the synthesis conditions, and a maximum hydration degree of about 90% (w/w) at room temperature.[6] Dynamic light scattering experiments showed an abrupt volume decrease of about 50% moving from 293 to 320 K for the microparticles with the highest content of NIPAAm and this temperature triggered shrinking can be used for an enhanced drug release at physiological temperature.[6]

The rationale behind the sensitivity to the temperature of the PVA-MA-NIPAAm microgel particles resides in the incorporation of oligo-*N*-isopropyl acrylamide sequences inside the covalent polymer scaffold, assuming that the network regions containing the *N*-isopropyl acrylamide residues maintain the thermosensitivity of p(NIPAAm). The transition from a relaxed, swollen state to a collapsed state of the polymer chains including NIPAAm should therefore determinate the deswelling of the microgel at a temperature near to the p(NIPAAm) LCST. The aim of the present investigation is to support this hypothesis with a description at a molecular level of the network behavior and of the polymer−water interaction, in view of an optimization of the structural and dynamical properties of the system as a device for controlled drug delivery. A simulation study of the PVA-MA-NIPAAm hydrogel has, moreover, an intrinsic interest, since it tackles aspects ranging from the modulation of hydrophilic/hydrophobic character of a polymer matrix by temperature and residue composition, to the polymer-induced modifications on the structure and dynamics of water. We approached the problem by molecular dynamics (MD), a consolidated tool in the study of protein dynamics and, in recent years, also used for simulating polymer systems, both in bulk and in solution.[29−35] A few MD simulations of poly(vinyl

* Corresponding author. E-mail: ester.chiessi@uniroma2.it.

10.1021/jp912209z
Published on Web 06/03/2010

CHART 1: Representation of the Junction in a PVA-MA-NIPAAm Microgel

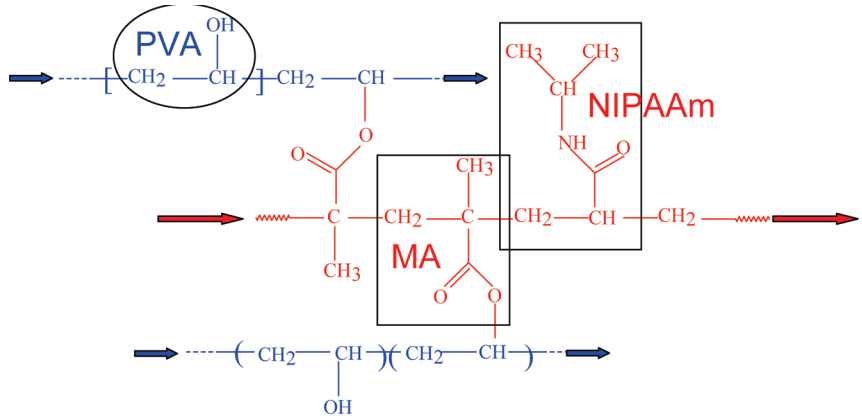

alcohol) (PVA) in aqueous solution are described in the literature,[36−41] and, recently, we reported an MD study of chemically cross-linked PVA hydrogels at high hydration degree, with a good agreement between experimental and simulation results.[42] Although many experimental works have been performed to characterize the volume phase transition of p(NIPAAm),[17,19−25] the simulation studies of this phenomenon are scarce. To our knowledge, only Tanaka et al,[36,37] Fornili et al,[43] and Gangemi et al[44] have reported on MD simulations of NIPAAm oligomers in water, showing a temperature dependence of the chain conformation. In the present paper we describe the results of an MD simulation study of two topologically different models of the junction domain of the PVA-MA-NIPAAm microgel at two temperatures, below and above the transition temperature. The hydration degree, the residue composition, and sequence were set in agreement with the experimental values, for a realistic representation of the system. For a better understanding of the results, we also performed comparative MD simulations of NIPAAm oligomers with two polymerization degrees in aqueous solution. The homopolymer systems provided a force-field validation and a reference behavior for the thermosensitivity.

2. Methods

2.1. Developing the Model. The covalent network of the PVA-MA-NIPAAm microgel, shown schematically in Chart 1, has a heterogeneous distribution of the residues in the chains, since the polymer scaffold is formed by PVA and poly(methacrylate-*co*-*N*-isopropyl acrylamide) (P(MA-NIPAAm)) segments. This is a consequence of the synthesis procedure of the microparticles, a photoinitiated free radical polymerization of methacryloyl-grafted PVA chains in aqueous solution in the presence of NIPAAm monomers.[6] A methacryloyl derivative of PVA, PVA-MA, is the starting polymer material and the three-dimensional network is the result of the polymerization reaction between methacryloyl groups and NIPAAm monomers, producing p(MA-NIPAAm) copolymer chains. The p(MA-NIPAAm) segments (shown in red in Chart 1) are the structural elements connecting the different PVA chains (shown in blue in Chart 1) in a network, and they also contain the residues imparting the thermosensitivity. The experimental characterization of the microparticles provided the MA/NIPAAm residue composition, that is, 1/2.5 in the system with the highest thermoresponsitivity, but, at the present, information about the average degree of polymerization (DP) of the p(MA-NIPAAm) segments is lacking. The PVA-MA-NIPAAm microparticles were obtained by PVA-MA with a degree of substitution (DS) of methacryloyl groups equal to 5%, corresponding to an average DP of 20 for the PVA segments between cross-links and to a PVA/MA/NIPAAm residue ratio of 20/1/2.5 in the final network. Accordingly to the previous considerations, we built two models for the junction domain of the network, both with 160 PVA, 8 MA, and 20 NIPAAm residues, but differing in the DP of the p(MA-NIPAAm) segments and in the distribution of the PVA chains, to test the effect of these structural parameters. In the first model, named PMN-I, a single segment of p(MA-NIPAAm), formed by 28 residues, connects 8 PVA chains, each of 20 residues. In the second model, named PMN-II, two segments of p(MA-NIPAAm), each formed by 14 residues, connect the 8 PVA chains, and two PVA chains from different p(MA-NIPAAm) segments are covalently bound (see Chart 2). For both models, the sequence of the residues in p(MA-NIPAAm) was randomly set, a more realistic description that any "block" distribution, taking into account the synthesis procedure.[6] The stereochemistry of the PVA and p(MA-NIPAAm) units was randomly assigned, with an equal contribution of R and S configurations. The initial structures were obtained using a program for molecular building of the CHARMM software package,[45] starting from the internal coordinates of the residues. The conformation of the chains in the initial structures was approximately all-trans. The structures were energy minimized in vacuo using the steepest descent method (about 2800 steps) with a maximum step size of 0.01 nm and a tolerance of 60 kJ·mol^{-1}·nm^{-1}, followed by 3000 steps of a conjugate gradient procedure with a tolerance of 4 kJ·mol^{-1}·nm^{-1}, with the force field used in the MD (see section 2.2). Another important aspect for a realistic simulation of these systems is the hydration degree, since the modulation of the water−polymer and polymer−polymer interactions is related to the polymer concentration. The starting structures were hydrated with an amount of water corresponding to the experimental polymer volume fraction, Φ_2, of about 0.10. Finally, the systems were compressed to the correct final density by means of preliminary MD simulations applying a "pressure bath" of 1 atm with the Berendsen's pressure coupling algorithm[46] at 323 K, a procedure already used for the simulation of PVA hydrogel networks.[42] The total trajectory time for the equilibration of the density was 350 ps. In the resulting configurations, the simulation boxes (cubic, with size of about 5.4 nm) contained a polymer network of 160 PVA, 8 MA, and 20 NIPAAm residues, hydrated by about 5200 water molecules for a polymer concentration of about 9% (w/w), with a density of 0.97 g/cm^3 at 323 K. The detailed description of the models and of the systems studied is reported in Part 1 of the Supporting

CHART 2: Topology and Residue Composition of Models

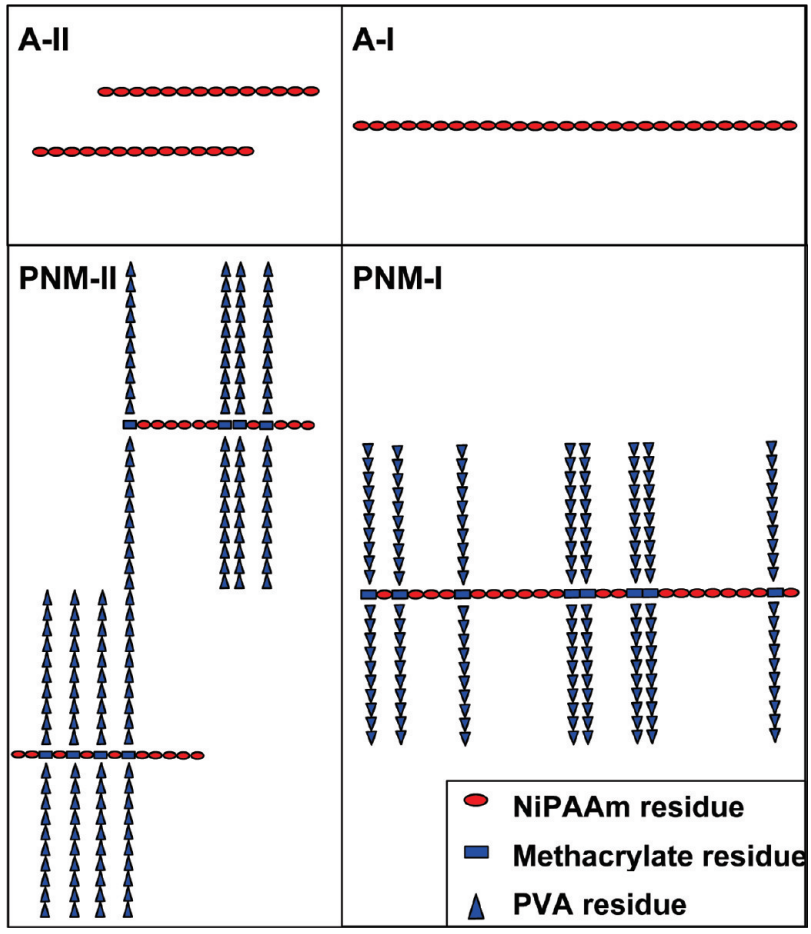

Information. We also performed comparative MD simulations on p(NIPAAm) oligomers in aqueous solution, using the same polymer concentration. The systems considered are a 28-unit oligomer and two 14-mer NIPAAm oligomers, named A-I and A-II, respectively, corresponding, in terms of the DP and the sequence of residue configuration, to the p(MA-NIPAAm) backbone of the PMN-I and PMN-II models (see Chart 2). The hydrated structures of A-I and A-II were obtained as described for the PVA-MA-NIPAAm systems.

2.2. Simulation Details. The preparation of the structures and part of the trajectory analysis were carried out by Compaq Alpha XP1000 and HP XW8600 workstations. MD simulations were performed on the IBM BladeCenter LS21 Cluster at the CINECA Supercomputing Center (Bologna, Italy) with the GROMACS 3.3.3 program.[47,48] The GROMOS 45A3 force field[49,50] was used, and the 45A4 ethanol model[51] was considered for the atomic partial charges of PVA residues. Aliphatic CH, CH_2, and CH_3 groups were treated with the united-atom convention, and the SPC water model was applied.[52] The simulations were carried out in the NPT ensemble, with the leapfrog integration algorithm[53] using a 2-fs time step, cubic periodic boundary condition, and the minimum image convention. The SHAKE procedure[54] was applied to constrain all bond lengths with a relative geometric tolerance of 10^{-4}. The temperature was controlled by the Berendsen coupling algorithm[46] using a time constant of 0.1 ps, and the simulations were performed at 323 and 293 K. The pressure was maintained at 1.0 bar by weak coupling to a pressure bath[46] via isotropic coordinate scaling with a relaxation time of 0.5 ps. Electrostatic interactions were calculated using the particle-mesh Ewald method, and nonbonded interactions were accounted for within a cutoff of 1.4 nm.

The acquired trajectory, including the equilibration, was 51 ns at 323 K, then followed by 51 ns at 293 K for PMN-I and PMN-II and 18 ns at both temperatures for A-I and A-II. The last 5 ns trajectory was considered for analysis at each temperature.

The atomic coordinates were saved every 0.4 ps and, for the last ns, every 0.2 ps to investigate the water properties and the polymer−solvent interaction.

A further test to verify the reproducibility of the results obtained with the PMN-I model of the PVA-MA-NIPAAm hydrogels was performed. The PMN-I system in the configuration at the end of the trajectory at 293 K was subjected to a simulating annealing, increasing the temperature to 373 K in 10 ns and decreasing to 323 K in 13 ns. A subsequent 20 ns trajectory at 323 K was then calculated and analyzed.

The hydrogen bond (HB) formation was monitored by analyzing the trajectory for the occurrence of this interaction, adopting as geometric criteria an acceptor−donor distance (A···D) lower than 0.35 nm and an angle Θ (A···H−D) higher than 120°. The time evolution of this interaction was studied by the time autocorrelation function of the HBs, $C_{HB}(t)$, calculated considering that the same HB can be interrupted at some intermediate time ("intermittent" $C_{HB}(t)$).[55−58] The correlation time, obtained by integrating $C_{HB}(t)$ in a range including the complete decorrelation ($C_{HB}(t) \leq 0.01$), was used as an estimate of the average lifetime of the HB. The water diffusion coefficient, D, was obtained from the long-time slope of the mean square displacement (MSD), according to eq 1:

$$D = \frac{1}{6}\lim_{t\to\infty}\frac{d}{dt}\langle|\mathbf{r}(t) - \mathbf{r}(0)|^2\rangle \quad (1)$$

where $\mathbf{r}(t)$ and $\mathbf{r}(0)$ correspond to the position vector of the water oxygen at time t and 0, respectively, with an average performed over both time origins and water molecules.[59] To evaluate the limiting slope, the time-window where the slope of log(MSD) versus log(t) approached unity was considered, typically about 20 ps.

The value and the range of confidence of the calculated properties were obtained by performing an average on the values calculated in several time windows selected in the last 5 ns trajectory.

An SPC water box of the same size as the PMN-I model was considered to simulate the bulk water properties for a comparison. A total trajectory of 1 ns at each temperature was calculated for bulk water.

The graphic visualization was done by the molecular viewer software package VMD.[60]

3. Results and Discussion

3.1. P(NIPAAm) Oligomers. The MD study of p(NIPAAm) oligomers in aqueous solution (models A-I and A-II) was performed to test the simulation protocol and it was helpful to define the computational "observables" evidencing the thermoresponsivity. Experimental results show that the LCST of p(NIPAAm) depends both on the DP and on the concentration of the polymer.[25,28] The phase transition can be observed in aqueous solutions of oligomers with at least three NIPAAm repeating units, and the LCST increases at decreasing DP and polymer concentration. For systems corresponding to models A-I and A-II the LCST, evaluated from turbidity measurements, is around to 302 and 313 K, respectively.[28] At temperatures higher than the LCST, the hydrophobic character of the polymer is dominant, and the increasing of the turbidity of the aqueous phase is due to aggregation and precipitation. In our simulation we calculated MD trajectories at 293 and 323 K for each model using the same initial configuration, expecting, at the highest temperature, a conformational response to the increased hydrophobicity and eventually an aggregation of the chains, in the case of model A-II. A temperature-induced modification of the conformation was found by Gangemi et al[44] in the MD study of a 26 unit oligomer of p(NIPAAm), using an AMBER forcefield. Figure 1 shows the time behavior of the radius of gyration, R_g, of A-I and the two A-II chains, calculated including only the backbone carbon atoms. After about 1.5 ns of trajectory at 323 K, the R_g of the 28-mer displays a sharp decrease, corresponding to a conformational transition to a coiled state, that persists for the following simulation time. The R_g of the same oligomer at 293 K maintains a value about twice that at 323 K after the transition (see Part 2 of the Supporting Information). The R_g's of the two 14-mers (Figure 1B,C) become stable after a longer trajectory time at both temperatures and the values at the highest temperature are only 10% lower than the corresponding at 293 K. The less marked difference in the conformation behavior of the shorter chains between the two temperature can be explained by considering that the LCST of these oligomers is near the highest temperature of our simulation and that the transition develops in a larger temperature interval.[28]

With the aim to highlight the chain regions involved in the aggregation, we calculated the matrix of the smallest average distances between couples of repeating units. The contact maps of Figure 2 were obtained with a time average on the last 5 ns trajectory and a color scale is used to indicate the distance value.

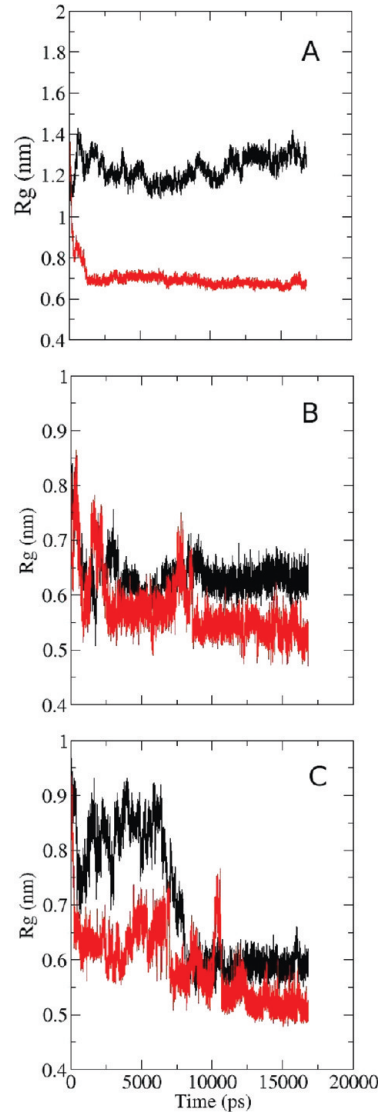

Figure 1. Radius of gyration of the p(NIPAAm) oligomers as a function of the trajectory time, at 293 K (black line) and 323 K (red line). (A) A-I chain. (B,C) A-II chains. Only the backbone carbon atoms were considered.

The difference between the left and right top matrices of Figure 2 documents the temperature effect on the conformation of the longer oligomer, which moves from an almost extended conformation at 293 K to a coiled state. A small increase in the number of intrachain contacts with the temperature for the shorter oligomers can be noted by comparing the left and right bottom matrices of Figure 2, but an increase of interchain aggregation is not observed. The time behavior of other properties, such as root-mean-square deviation, end-to-end distance, and the radial distribution functions between the backbone C atoms, (data not shown) confirm the modification of the chain conformation by temperature. Some average structural data of the systems, calculated on the last 5 ns trajectory at the two temperatures, and a figure showing the final configuration of A-I at the two temperatures are reported in Parts 2 and 3, respectively, of the Supporting Information.

The mobility of the chains was evaluated by calculating the root-mean-square fluctuation (RMSF) of atomic positions for each backbone carbon atom:

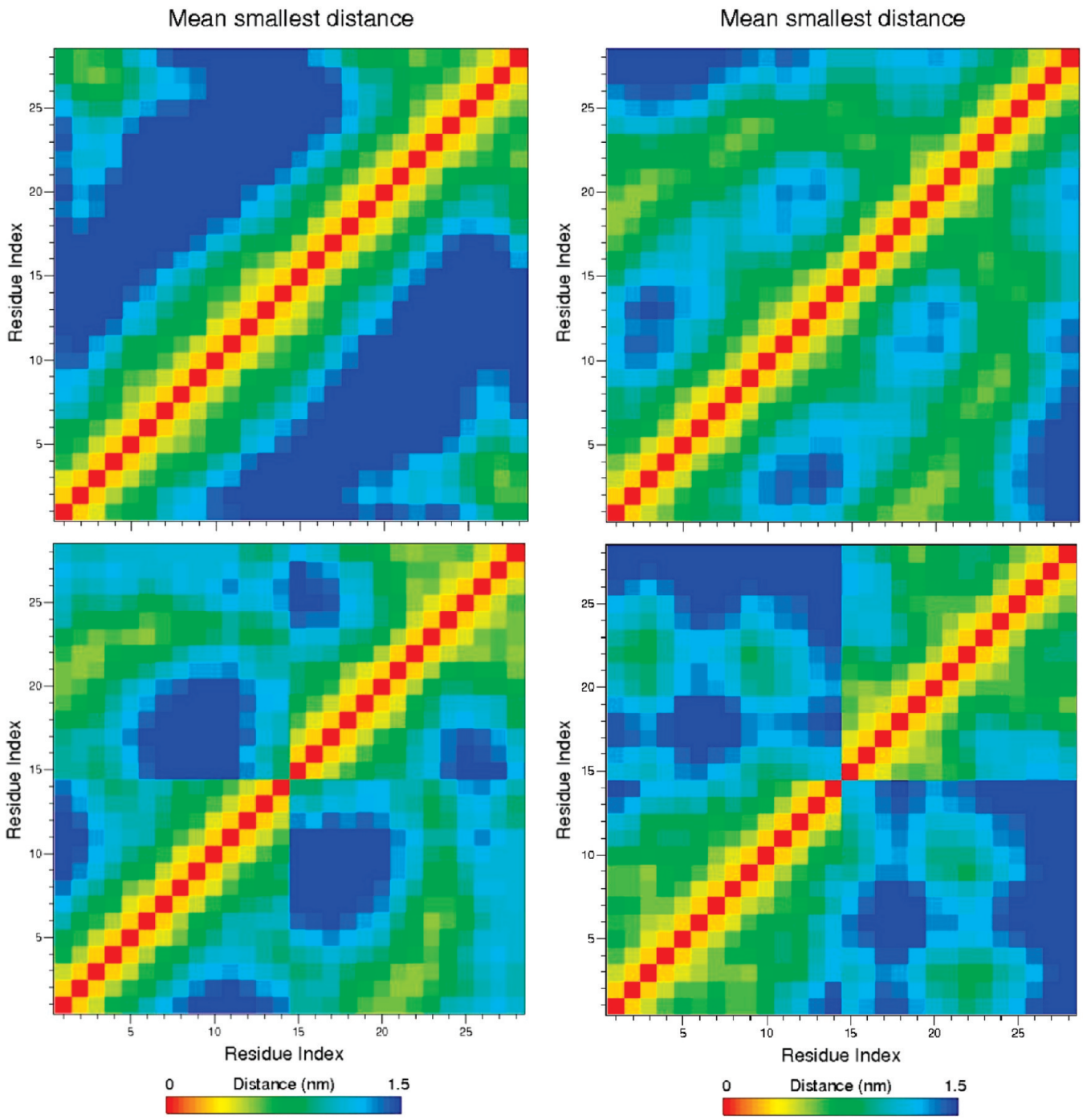

Figure 2. Matrices of the smallest average distances between couples of repeating units for A-I (top) and A-II (bottom) systems, at 293 K (left matrices) and 323 K (right matrices). Time average in the last 5 ns trajectory. The color coding indicates the distance values.

$$\mathrm{RMSF}_i = \sqrt{\langle(\mathbf{r_i}(t) - \langle\mathbf{r_i}\rangle)^2\rangle_t} \qquad (2)$$

in the time interval of the last 5 ns. The ensemble averaged values are reported in Table 1. The RMSF is related to the X-ray diffraction B-factor[61] and an increase with the temperature is the expected behavior. Therefore it is noteworthy that the average RMSF of the A-I chain is unaffected by temperature, since at the highest temperature the intramolecular interactions in the folded conformation compensate the increased thermal agitation. One of the two chains of the model A-II shows a behavior of RMSF with temperature similar to that of A-I, while the other chain displays the expected trend.

The structure and dynamics of a macromolecule are strictly related to the interactions established between the chain residues and between chain residues and water molecules. We analyzed the hydrogen bonding in the systems, and the results are reported in Table 2. On average, one intramolecular HB every seven

TABLE 1: Root Mean Square Fluctuations[a]

system	RMSF (nm) at 293 K	RMSF (nm) at 323 K
A-I	0.15 ± 0.03	0.13 ± 0.04
A-II	0.05 ± 0.02	0.10 ± 0.04
	0.05 ± 0.02	0.06 ± 0.02
PMN-I	0.06 ± 0.02	0.06 ± 0.02
PMN-II	0.04 ± 0.02	0.08 ± 0.03
	0.04 ± 0.01	0.07 ± 0.04

[a] Ensemble averaged values. RMSF's were calculated in the last 5 ns trajectory after roto-traslational fit.

TABLE 2: Polymer−Polymer and Polymer−Water Hydrogen Bonding[a]

system		293 K		323 K	
		average HB number per residue and HB lifetime[b](ps)		average HB number per residue and HB lifetime[b](ps)	
		polymer−polymer	polymer−H_2O	polymer−polymer	polymer−H_2O
A-I		0.14 ± 0.05	1.32 ± 0.01 (17 ± 1)	0.22 ± 0.06	0.93 ± 0.03 (12 ± 2)
A-II		0.17 ± 0.05	1.01 ± 0.03 (18 ± 2)	0.14 ± 0.05	1.10 ± 0.02
PMN-I	MA-NIPAAm	0.08 ± 0.03	0.55 ± 0.02	0.09 ± 0.04	0.36 ± 0.06
	PVA	0.39 ± 0.03	0.97 ± 0.02	0.36 ± 0.03	0.93 ± 0.01 (9.0 ± 0.7)
PMN-II	MA-NIPAAm	0.02 ± 0.02	0.62 ± 0.02 (33 ± 6)	0.04 ± 0.03	0.52 ± 0.06 (16 ± 3)
	PVA	0.43 ± 0.03	0.78 ± 0.03 (21 ± 3)	0.40 ± 0.03	0.72 ± 0.07 (9.8 ± 0.9)

[a] Analysis performed on the last 5 ns trajectory. [b] HB lifetime was evaluated when a complete decay of the corresponding HB autocorrelation function was found. Values of HB lifetimes are reported in parentheses.

NIPAAm residues at 293 K was found for both systems. In the case of the 28-mer at the highest temperature, the average number of intramolecular HB's increases and, correspondently, the number of HB's with water decreases. This result is in agreement with the conformational modification of the chain and explains the lacking increase of the RMFS. For the A-II system, the average HB number between NIPAAm residues does not change with the temperature (columns 2 and 4 of Table 2). However, at 293 K, these HB's are mostly formed between different chains, while at 323 K they are mostly intrachain, as confirmed by the bottom maps of Figure 2, in agreement with a coiling of the chains. A dynamic information is provided by the average HB lifetimes, τ_{HB}, obtained by integration of the time autocorrelation function, $C_{HB}(t)$. The τ_{HB} for the polymer−water HBs, of about 18 ps for both models at 293 K, estimates an average time for the exchange of the water molecules in the first hydration shell. A decrease of this τ_{HB} between 293 and 323 K was observed in A-I, while the corresponding evaluation for A-II was not possible for the presence of stable polymer−water HBs, hindering the complete decay of the $C_{HB}(t)$.

3.2. PVA-MA-NIPAAm Systems. In the trajectory analysis we searched a conformational modification related to the temperature variation for the systems PMN-I and PMN-II, representing a model of the junction domain in the polymer matrix of PVA-MA-NIPAAm microgels. The chemical heterogeneity of the network, formed by PVA chains, prevalently hydrophilic, and methacrylate-*co*-NIPAAm chains, with a temperature tunable hydrophobicity, determinates a possible different behavior of the corresponding regions. In the topology of the polymer scaffold, the methacrylate-*co*-NIPAAm segments form the cross-linking backbone for the PVA chains (see Chart 2). The conformation of these backbone chains, containing the thermoresponsive residues, was investigated following the time behavior of the radius of gyration, $R_{g,MN}$, calculated including only the 56 carbon atoms of the methacrylate-*co*-NIPAAm segment. As reported in Figure 3, the $R_{g,MN}$ of the 28-unit chain shows a sharp decrease during the trajectory at the highest temperature and settles down, in the last 5 ns, at a value about 20% lower than the corresponding at 293 K. The comparison with the results obtained for the A-I model (Figure 1 and Part 2 of the Supporting Information) suggests that the sensitivity to the temperature of the NIPAAm oligomer is also maintained in the copolymer segment of PMN-I, taking into account that the volume excluded effect and the topological constraint of the PVA chains prevent a decreasing of $R_{g,MN}$ up to the value obtained for A-I. The dependence on the temperature of the time averaged $R_{g,MN}$ value for the two PMN-II chains is less marked when compared with the corresponding NIPAAm oligomers (Part 2 of the Supporting Information). The $R_{g,MN}$ values in PMN-II are, moreover, higher than those in A-II at all temperatures.

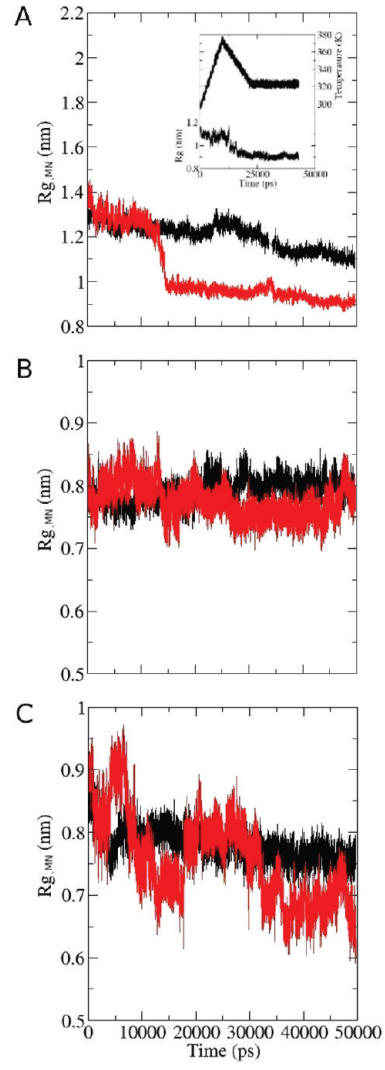

Figure 3. Radius of gyration of the (MA-NIPAAm) chains as a function of the trajectory time, at 293 K (black line) and 323 K (red line). A: PMN-I system. B and C: PMN-II system. Only the backbone carbon atoms were considered. Inset of A: Radius of gyration of the (MA-NIPAAm) chain in PMN-I and temperature during and after the simulated annealing.

The matrixes of the smallest average distances between couples of repeating units of the methacrylate-*co*-NIPAAm sequence for PMN-I and PMN-II, time averaged in the last 5 ns trajectory, are shown in Figure 4. A chain rearrangement, corresponding to a more coiled conformation, can be noted at 323 K only for PMN-I. For PMN-II, the map at the highest temperature shows a decreased number of interchain contacts. Also the behavior of the ensemble averaged RMSFs of the

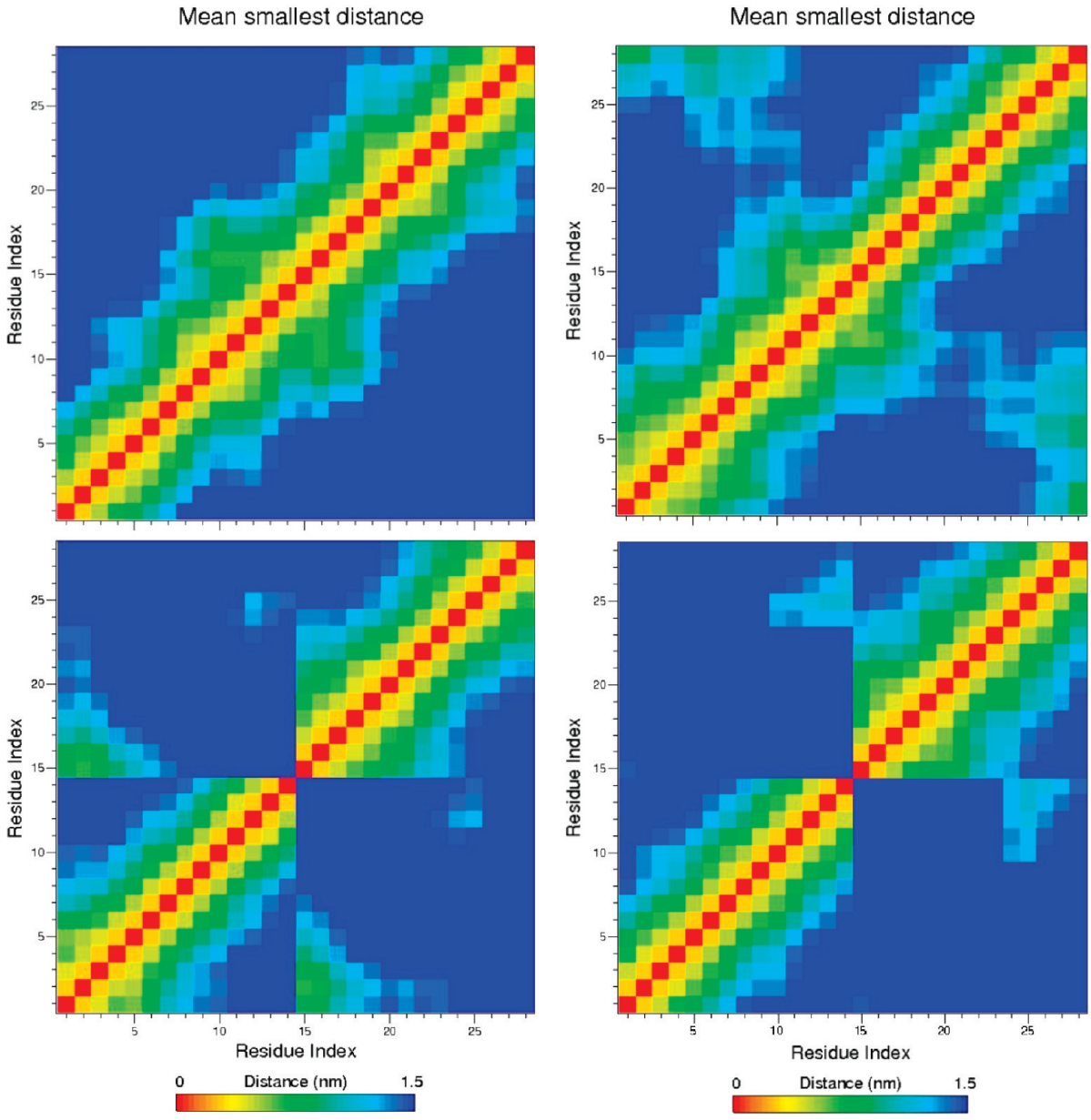

Figure 4. Matrices of the smallest average distances between couples of repeating units for the MA-NIPAAm chains in PMN-I (top) and PMN-II (bottom) systems, at 293 K (left matrices) and 323 K (right matrices). Time average in the last 5 ns trajectory. The color coding indicates the distance values.

NIPAAM-containing backbone, reported in Table 1, confirms the analogy between the cross-linking chain of PMN-I and the A-I chain. The RMSF values of PMN-I are obviously lower than those of A-I, for the restraining effect of the PVA, but, as for A-I, they do not increase with the temperature. The picture of a hydrophobic collapse at the highest temperature is supported by the analysis of the radial distribution function between backbone carbon atoms and the water oxygen atom, $g_{C\text{-}OW}(r)$, shown in Figure 5. The $g_{C\text{-}OW}(r)$ for PMN-I and A-I at 323 K is lower than the corresponding $g_{C\text{-}OW}(r)$ at 293 K in a spatial domain larger than the average radius of gyration. This result indicates a lower hydration degree in the surrounding of the NIPAAm containing chains at the highest temperature, and it was not obtained for PMN-II (data not shown).

The reported results allow one to state that the methacrylate-*co*-NIPAAm chain with a DP of 28 is able to show a thermosensitivity similar to that of the corresponding NIPAAm oligomer, in spite of the methacrylate "defects" and the topological constraints of the PVA segments. The observed temperature effect on the backbone conformation in PMN-I was confirmed in a reproducibility test, described in section 2.2. Starting from the final configuration at 293 K, after a simulating annealing followed by an equilibration at 323 K, the system again assumes a coiled backbone conformation, as shown in the inset of Figure 3A.

The sensitivity to temperature of the backbone conformation is strongly dependent on the junction topology, since only in the PMN-I system was a thermoresponsivity effect observed. It is noteworthy that, in the methacrylate-*co*-NIPAAm chains of both models, at least one sequence containing at least three consecutive NIPAAm residues was present (see Chart 2), the minimum requirement in term of DP for the thermal sensitivity of the NIPAAm oligomers.[28] The different topology, moreover, causes a different dynamic behavior of water in the junction domain. In Figure 6 the autocorrelation functions, $C_{HB}(t)$, for the HBs formed between MA-NIPAAm residues and water are reported for both models. In the case of PMN-II, $C_{HB}(t)$ changes with the temperature according to the expected behavior, with

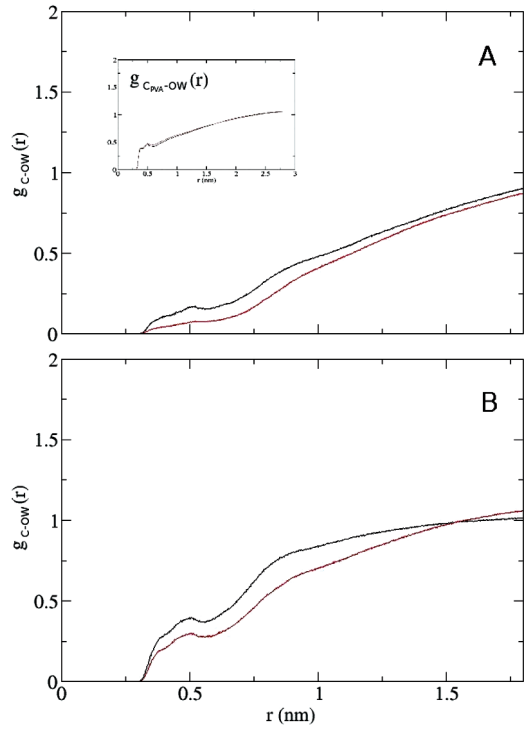

Figure 5. Radial distribution function between backbone carbon atoms and water oxygen atom, at 293 K (black line) and 323 K (red line). A: MA-NiPAAm chain in PMN-I. B: A-I chain. Inset of A: radial distribution function between PVA carbon atoms and water oxygen atoms, at 293 K (black line) and 323 K (red line).

a more rapid decrease at the highest temperature and a corresponding lower average HB lifetime. The semilogarithmic plot of $C_{HB}(t)$ for PMN-II (reported in Part 4 of the Supporting Information) shows a biphasic decay, indicating two differently bound water components, with characteristic times of tens and hundreds of picoseconds, both decreasing at increasing temperature. For PMN-I, the dependence of $C_{HB}(t)$ on temperature is opposite that of PMN-II, and a complete decay of $C_{HB}(t)$ was not observed at both temperatures, preventing an evaluation of the HB lifetime. The semilogarithmic plot of $C_{HB}(t)$ for PMN-I (reported in Part 4 of the Supporting Information) reveals a residual water component with the same behavior of the faster component in PMN-II, by comparing the time decay in the two models below 40 ps. However, the contribution of correlating HBs in PMN-I, corresponding to blocked water molecules, is evident and particularly relevant at 323 K, when the MA-NiPAAm chain is coiled. Therefore the crowding of the junction domain in PMN-I, due to the higher DP of the MA-NIPAAm cross-linking chain giving a higher local cross-linking density, produces the confinement of the surrounding water and the freezing of the diffusion motion for a few solvent molecules. The modification of dynamical behavior for water adsorbed on the surface of biological macromolecules was experimentally proved,[62] and a supercooling effect was reported for water in polymer hydrogels.[63] Moreover, a very slow water component in cells of a halophilic organism, with residence times of hundreds of picoseconds, was assessed by neutron scattering measurements.[64] According to these results, simulation studies described the polymer-induced slowing of water dynamics in hydrated networks[65,37,42] and at the protein−solvent interface,[66] showing an influence on the dynamical properties of solvent similar to that found in the models of the microgel junction reported in this paper.

The structural and dynamic properties of the PVA component were also investigated to evaluate the overall behavior of the PVA-MA-NIPAAm network. We found that the hydrophilic character of PVA is not affected by the temperature, as shown by the radial distribution function between PVA carbon and water oxygen atoms (inset of Figure 5 A), and by the average number of PVA-water HBs (Table 2), practically independent of temperature. The increase of temperature has a kinetic effect, with a faster renewal of the first hydration shell of PVA, as indicated by the HB lifetime values in Table 2.

The overall average dimension of the polymer system can be evaluated by the radius of gyration, $R_{G,TOT}$, calculated including also the PVA carbon atoms. The average value of this parameter is reported in Part 2 of the Supporting Information. We observed that $R_{G,TOT}$ is practically the same at the two temperatures for both models, since the conformational modification of the methacrylate-*co*-NIPAAm core in PMN-I is compensated by a larger extension of the PVA chains. Therefore the chemical heterogeneity of the network determinates a heterogeneity in the temperature-induced modifications of the chain conformation. These considerations are supported from the comparison between the final configurations of PMN-I system at 293 and 323 K, shown in Figure 7.

To study the effects of temperature on the polymer mobility we analyzed the torsional dynamics of the chains, governed by the possibility of transitions between different conformations of the dihedral angles. For an N residue linear vinyl polymer, $[2\cdot(N-2)+2]$ chain dihedrals are to be monitored, all equivalent in a homopolymer, to detect the transitions between rotational states. We found that the transitions occurred between the *trans* and *gauche* states, as the *cis* barrier was never crossed during our simulations, both for MA-NIPAAm and PVA chains.

An average lifetime of rotational state, $\langle\tau_{rot}\rangle$, was estimated by means of eq 3:

$$\langle\tau_{rot}\rangle = \frac{1}{N_{DIHE}}\sum_{i=1}^{N_{DIHE}}\frac{t_{TOT}}{(N_{TRANS,i}+1)} \qquad (3)$$

where N_{DIHE}, t_{TOT}, and $N_{TRANS,i}$ are the number of dihedral angles that perform transitions, the total simulation time, and the number of transitions of the ith dihedral angle, respectively. In eq 3, the single term of the summation represents the average lifetime of rotational state for the ith dihedral angle, $\tau_{rot,i}$, then the average is performed on mobile chain dihedral angles. The $\langle\tau_{rot}\rangle$ values and the fraction of mobile chain dihedral angles, obtained by separately considering the methacrylate-*co*-NIPAAm and PVA chains, are reported in Table 3, including also the corresponding data for the A-I and A-II models. The fraction of mobile dihedral angles for the PVA moiety is always higher than that of the methacrylate-*co*-NIPAAm and the oligo-NIPAAm chains, due to the larger sterical hindrance in the last systems. The MA-NIPAAm chains display a lower mobility than the PVA chains also considering $\langle\tau_{rot}\rangle$. The latter value is about 1 ns for the methacrylate-*co*-NIPAAm and oligo-NIPAAm segments and about a half nanosecond for the PVA at 293 K. It can be noted that the temperature increase affects the torsional dynamics both with an increase of the fraction of mobile dihedral angles and with a decrease of $\langle\tau_{rot}\rangle$. In PMN-I and PMN-II, the effect of the temperature on $\langle\tau_{rot}\rangle$, in terms of relative decrease, is more pronounced for the more hindered chains, i.e., the methacrylate-*co*-NIPAAm segments, than for PVA. It is noteworthy, moreover, that for the oligo-NIPAAm chains the

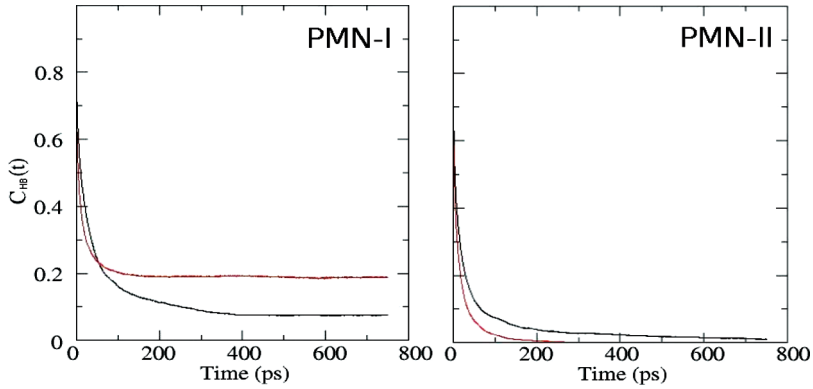

Figure 6. Autocorrelation function of the HBs between MA-NIPAAm residues and water, at 293 K (black lines) and 323 K (red lines).

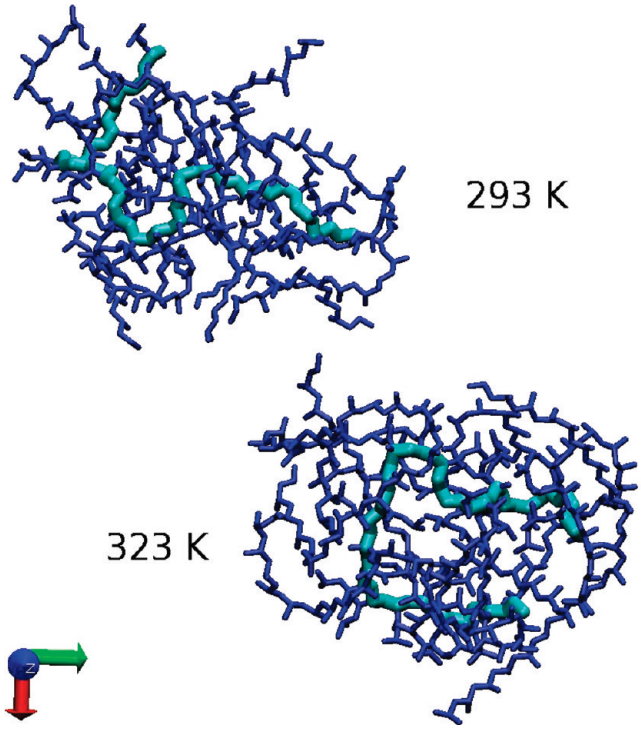

Figure 7. Projections in the *xy* plane of the final configuration of PMN-I. PVA and MA-NIPAAm chains are shown in blue and azure, respectively. Water molecules are not shown.

TABLE 3: Torsional Dynamics[a]

		293 K		323 K	
	system	fraction of mobile dihedrals	$\langle\tau_{rot}\rangle^b$ (ps)	fraction of mobile dihedrals	$\langle\tau_{rot}\rangle^b$ (ps)
	A-I	0.40	806 ± 111	0.70	568 ± 92
	A-II	0.30	966 ± 194	0.46	658 ± 122
PMN-I	MA-NIPAAm	0.13	911 ± 190	0.38	433 ± 88
	PVA	0.72	462 ± 17	0.95	269 ± 9
PMN-II	MA-NIPAAm	0.22	1056 ± 136	0.58	668 ± 96
	PVA	0.71	534 ± 19	0.91	344 ± 13

[a] Analysis performed on the last 5 ns trajectory. [b] Average lifetime of rotational state estimated by eq 3, with root-mean-square deviation.

"activation" of the torsional dynamics at the highest temperature is restrained by the conformational change.

The torsional mobility of PVA in these PVA-MA-NIPAAm networks is lower than in hydrogels formed by chemical cross-linking of PVA telechelic chains,[42] due to the more crowded assembly of the chains in the junction domain of the former systems in comparison with the three-functional junctions that connect chains in PVA hydrogels. In this respect, the higher local chain density also affects the water dynamics in the first hydration shell, determining a general increase of the polymer−water HB lifetimes, in comparison with PVA telechelic hydrogels,[65c] and the lack of a complete decay of the HB autocorrelation function at 293 K also for the PVA−water HBs in the PMN-I system (see Table 2).

3.3. Solvent Properties. In a process involving hydrophobic interactions water molecules play a key role, related to the rearrangement of the shell surrounding solutes and desolvation of interacting surfaces. The properties of water in a hydrophobic environment are differently affected depending on the dimension and the topology of the hydrophobic interface.[67−69] Experimental results indicate that the mobility of water molecules in solutions of apolar solutes is decreased,[70] in relation with a modification in water density around the interacting objects, and simulation studies were performed to describe at a molecular level this phenomenon.[71,72] Also the interaction with hydrophilic matrices causes a slowing of the water dynamics, as reported for polysaccharide and polymer hydrogels.[63a,73]

In the present work we investigated some structural and dynamic properties of water in the A and PMN systems, i.e., the hydrogen bonding and the self-diffusion coefficient, and we compared them with the corresponding properties of the bulk water. We used a similar approach in a previous MD study on PVA hydrogels, where a polymer-induced supercooling effect of water, in agreement with quasi-elastic incoherent neutron scattering results, was evidenced.[42]

In order to select the water according to the interactions with polymer chains, the solvent in the NIPAAm oligomer systems and in PVA-MA-NIPAAm models was sampled by considering a "close contact" (CC) domain, including the water molecules within a distance of 0.6 nm, and a second domain (farther, F), with the remaining molecules. The CC domain contained about 18% and 15% of the total water in the A and PMN systems, respectively, at both the temperatures. The average number of HBs formed between water molecules is lower in the CC domain than in the farthest region from the polymer, as reported in Table 4, and, also including the HBs with polymer groups, the water in a neighborhood within 0.6 nm from the polymer results less structurally organized than the bulk water. The extent of this effect is similar in the NIPAAm oligomer systems and in PVA-MA-NIPAAm models at both temperatures. For solvent molecules at distances greater than 0.6 nm, an opposite result was obtained, i.e., an average number of HBs per water molecule higher than in bulk. This indicates a rearrangement of water to optimize the intermolecular interaction, with differences between A and PMN systems within errors.

TABLE 4: Water Properties[a]

	293 K				323 K			
	average number of HB's per water molecule		D/D_0[b]		average number of HB's per water molecule		D/D_0[b]	
	domain[c]		domain[c]		domain[c]		domain[c]	
system	CC	F	CC	F	CC	F	CC	F
A-I	1.27 ± 0.03	1.65 ± 0.01	0.71 ± 0.09	0.97 ± 0.13	1.16 ± 0.03	1.58 ± 0.01	0.78 ± 0.09	0.98 ± 0.13
A-II	1.25 ± 0.03	1.65 ± 0.01	0.75 ± 0.09	0.97 ± 0.13	1.16 ± 0.01	1.58 ± 0.01	0.78 ± 0.08	0.97 ± 0.13
PMN-I	1.27 ± 0.02	1.68 ± 0.01	0.70 ± 0.09	0.99 ± 0.13	1.20 ± 0.02	1.61 ± 0.01	0.75 ± 0.10	0.97 ± 0.14
PMN-II	1.27 ± 0.02	1.67 ± 0.01	0.71 ± 0.09	0.98 ± 0.14	1.20 ± 0.02	1.60 ± 0.01	0.76 ± 0.10	0.97 ± 0.13
bulk	1.52 ± 0.02		1		1.45 ± 0.02		1	

[a] Analysis performed on the last nanoseconds, with an average over 10 configurations. [b] D_0 is the diffusion coefficient from the simulation of bulk water. [c] CC domain includes water molecules at distances lower than 0.6 nm from the polymer; F domain includes the remaining water molecules.

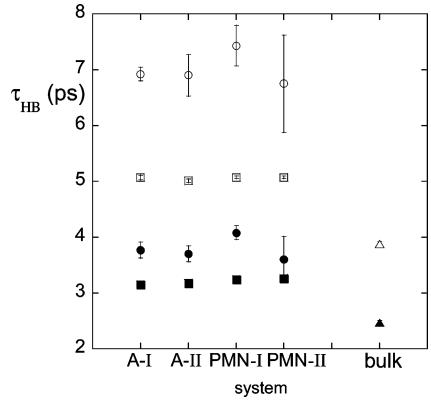

Figure 8. Average lifetime of the HBs between water molecules in the different systems. Circles: CC domain; squares: F domain. Triangles: bulk water values. Open symbols: 293 K; filled symbols: 323 K.

The average lifetime of the HBs between water molecules (τ_{HB}), evaluated by the "intermittent" HB autocorrelation function,[55−58] estimates the average contact persistence for a pair of water molecules. The τ_{HB}'s, calculated for the two water domains, are shown in Figure 8 with the corresponding values for bulk water. Figure 8 indicates a strong slowing in the CC domain, where the water dynamics is coupled with the desolvation process, characterized by times of tens of picoseconds (see Table 2). The solvent dynamics in the F regions is also affected, in agreement with the structural effect indicated by the increased average number of HBs.

The self-diffusion coefficient is a dynamic property of water, experimentally accessible by means NMR relaxation spectroscopy[74] and incoherent quasi-elastic neutron scattering (QENS).[75] The average D value of water molecules in different domains was obtained using the Einstein relation[59] (eq 1 in section 2.2) and the relative values, D/D_0, with D_0 being the diffusion coefficient obtained from the simulation of bulk water, are reported in Table 4. The time-window used to evaluate the MSD limiting slope for water molecules in the CC domain was shorter than the average lifetime of oligomer-water HBs, to prevent the selected solvent molecules from moving away from the oligomer proximity region. The water molecules in the CC domain display a decreasing D of about 29% and 23% with respect to the bulk water, at 293 and 323 K, respectively, while for the remaining water the average D value is similar to that of bulk water. The differences between the A and PMN systems are within errors. Shibayama et al[76] recently determined a drop of the water diffusion coefficient in p(NIPAAm) solutions with a polymer concentration of about 27% (w/w), using QENS experiments. Their data show a decrease of about 38% and 24% with respect to the bulk value, at 293 and 318 K, respectively. In a QENS study on PVA hydrogels at high hydration degree,[63a] we reported a decrease of about 33% and 32% at 293 and 323 K, respectively, for the D of the slowly relaxing water. The decrease of D obtained for the PMN systems is in a satisfactory agreement with that observed in PVA hydrogels and in p(NIPAAm) aqueous solutions, at both temperatures. These results indicate that the increase of the hydrophobic character cannot be discriminated by an effect on the water self-diffusion coefficient, since the polymer-induced modification of water D is similar between a hydrophilic and a hydrophobic matrix.[71] The apparent contradiction between the behavior of τ_{HB}, higher than that of bulk water, and that of D, similar to the bulk value, observed for the water molecules in the F domain, can be explained by considering the relation between these two parameters. In a domain far from the polymer, the water translational motion can be represented with a set of uncorrelated jumps from one site to another, and several jumps occur before the definitive departure of two water molecules. This behavior corresponds to the description provided by the "random jump" model,[77] where D is related to the average length of a jump, l, and to the residence time in a site, $\tau^{\#}$, by eq 4:

$$D = \frac{l^2}{6\tau^{\#}} \tag{4}$$

The τ_{HB} value represents the time interval inside which a particular couple of water molecules is found to form an HB, and it can be longer than $\tau^{\#}$, depending on the number of jumps performed from the first HB event between the two molecules (at t_0) to the last HB event (at $t_0 + \tau_{HB}$). The inspection of the radial distribution functions between oxygen atoms in bulk water and in the water of the F domain (not shown) indicates that there are no differences in the distance distribution respect to bulk water and this result suggests a similar l value. We can therefore conclude that the water diffusion in regions at distances from the polymer longer than 0.6 nm does not differ from bulk water, in terms of the D, l, and $\tau^{\#}$ parameters, but it happens with a different pattern determining a higher τ_{HB} value.

Our results indicate that the interaction with the PVA-MA-NIPAAm network produces a rearrangement in the HB distribution and a slowing of the water dynamics, and that these effects are less marked at the highest temperature and independent of the network topology. These characteristics are relevant for the use of the microgel as a drug release device, considering that the drug diffusion is related to that of water molecules.

Concluding Remarks

The present study provided a molecular description of the junction domain for the polymer network of PVA-MA-NIPAAm microgels in agreement with the experimentally observed thermoresponsitivity. The DP of the MA-NIPAAm cross-linking chain was found to be a key parameter in order that the temperature effect on the conformation of the NIPAAm-containing chain could be detected, and this suggests a large heterogeneity in the network mesh size, particularly above the transition temperature, due to the polydispersity of the P(MA-NIPAAm) segments. The simulation results describe the thermoresponsivity of the PVA-MA-NIPAAm microgel in terms of a modification of the internal texture of the network, with an alteration of the pore size distribution and a limited variation of the hydration degree. The water dynamics in the microparticles is affected with a slowing effect, less marked at the highest temperature, corresponding to the condition for the drug release in the physiological environment. This result was confirmed by QENS experiments, whose results will be reported in a forthcoming paper.[78] A larger network model is under study, for a coarse-grained simulation probing of the distribution of the mesh size at the nanoscale, to compare with confocal laser scanning microscopy and X-ray microspectroscopy results.

Acknowledgment. This work was partially funded by MIUR project PRIN 20077LCNTW_003. The authors thank CNISM/CINECA for supplying high performance computing facilities.

Supporting Information Available: Part 1, a table with the details of the structural characteristics of the models. Part 2, a table with the average backbone conformational properties. Part 3, a figure with the comparison between the final configurations of A-I at 293 and 323 K. Part 4, a semilogarithmic plot of the autocorrelation functions of the HB's between MA-NIPAAm residues and water. This information is available free of charge via the Internet at http://pubs.acs.org.

References and Notes

(1) Klouda, L.; Mikos, A. G. *Eur. J. Pharm. Biopharm.* **2008**, *68*, 34–45.
(2) Bonacucina, G.; Cespi, M.; Misici-Falzi, M.; Palmieri, G. F. *J. Pharm. Sci.* **2009**, *98*, 1–42.
(3) Yu, L.; Ding, J. *Chem. Soc. Rev.* **2008**, *37*, 1473–81.
(4) Hendrickson, G. R.; Lyon, L. A. *Soft Matter* **2009**, *5*, 29–35.
(5) Cavalieri, F.; Chiessi, E.; Villa, R.; Vigano', L.; Zaffaroni, N.; Telling, M. F. *Biomacromolecules* **2008**, *9*, 1967–1973.
(6) Ghugare, S. V.; Mozetic, P.; Paradossi, G. *Biomacromolecules* **2009**, *10*, 1589–1596.
(7) Saunders, B. R.; Laajam, N.; Daly, E.; Teow, S.; Hu, X.; Stepto, R. *Adv. Colloid Interface Sci.* **2009**, *147*, 251–62.
(8) Olea, A. F.; Rosenbluth, H.; Thomas, J. K. *Macromolecules* **1999**, *32*, 8077–8083.
(9) Paradossi, G.; Cavalieri, F.; Chiessi, E.; Ponassi, V.; Martorana, V. *Biomacromolecules* **2002**, *3*, 1255–1262.
(10) Karg, M.; Pastoriza-Santos, I.; Rodriguez-Gonzlez, B.; von Klitzing, R.; Wellert, S.; Hellweg, T. *Langmuir* **2008**, *24*, 6300–6306.
(11) Bluestone, S.; Mark, J. E.; Flory, P. J. *Macromolecules* **1974**, *7*, 325–30.
(12) Bailey, F. E.; Powell, G. M.; Smith, K. L. *Ind. Eng. Chem.* **1958**, *50*, 8–11.
(13) Tsuboi, Y.; Yoshida, Y.; Okada, K.; Kitamura, N. *J. Phys. Chem. B* **2008**, *112*, 2562–2565.
(14) Lu, X.; Hu, Z.; Gao, J. *Macromolecules* **2000**, *33*, 8698–8702.
(15) Choi, S. H.; Lee, J. H.; Choi, S. M.; Park, T. G. *Langmuir* **2006**, *22*, 1758–1762.
(16) Ueki, T.; Watanabe, M. *Langmuir* **2007**, *23*, 988–990.
(17) Schild, H. G. *Prog. Polym. Sci.* **1992**, *17*, 163–249.
(18) Heskins, M.; Guillet, J. E. *J. Macromol. Sci., Chem.* **1968**, *A2*, 1441–1455.
(19) Fujishige, S.; Kubota, K.; Ando, I. *J. Phys. Chem.* **1989**, *93*, 3311–3313.
(20) Schild, H. G.; Tirrel, D. A. *J. Phys. Chem.* **1990**, *94*, 4352–4356.
(21) Shirota, H.; Kuwabara, N.; Ohkawa, K.; Horie, K. *J. Phys. Chem. B* **1999**, *103*, 10400–10408.
(22) Dhara, D.; Rathna, G. V. N.; Chatterji, P. R. *Langmuir* **2000**, *16*, 2424–2429.
(23) Tsuboi, Y.; Yoshida, Y.; Okada, K.; Kitamura, N. *J. Phys. Chem. B* **2008**, *112*, 2562–2565.
(24) Tanaka, F.; Koga, T.; Winnik, F. M. *Phys. Rev. Lett.* **2008**, *101*, 028302 [1−4].
(25) Pamies, R.; Zhu, K. Z.; Kjøniksen, A. L.; Nyström, B. *Polym. Bull.* **2009**, *62*, 487–502.
(26) Yoshida, R.; Kokufuta, E.; Yamaguchi, T. *Chaos* **1999**, *9*, 260–266.
(27) Wei, H.; Yu, H.; Zhang, A. Y.; Sun, L. G.; Hou, D.; Feng, Z. G. *Macromolecules* **2005**, *38*, 8833–8839.
(28) Shan, J.; Zhao, Y.; Granqvist, N.; Tenhu, H. *Macromolecules* **2009**, *42*, 2696–2701.
(29) Tasaki, K. *J. Am. Chem. Soc.* **1996**, *118*, 8459–8469.
(30) Borodin, O.; Bedrov, D.; Smith, G. D. *J. Phys. Chem. B* **2002**, *106*, 5194–5199.
(31) Bedrov, D.; Smith, G. D. *Langmuir* **2006**, *22*, 6189–6194.
(32) Hess, B.; Sayar, M.; Holm, C. *Macromolecules* **2007**, *40*, 1703–1707.
(33) Wu, Y. B.; Joseph, S.; Aluru, N. R. *J. Phys. Chem. B* **2009**, *113*, 3512–3520.
(34) Gotlib, I. Y.; Piotrovskaya, E. M.; de Leeuw, S. W. *J. Phys. Chem. C* **2007**, *111*, 6613–6620.
(35) Tanis, I.; Tragoudaras, D.; Karatasos, K.; Anastasiadis, S. H. *J. Phys. Chem. B* **2009**, *113*, 5356–5368.
(36) Tamai, Y.; Tanaka, H.; Nakanishi, K. *Macromolecules* **1996**, *29*, 6750–6760.
(37) Tamai, Y.; Tanaka, H.; Nakanishi, K. *Macromolecules* **1996**, *29*, 6761–6769.
(38) Tamai, Y.; Tanaka, H. *Chem. Phys. Lett.* **1998**, *285*, 127–132.
(39) Tamai, Y.; Tanaka, H. *Fluid Phase Equilib.* **1998**, *144*, 441–448.
(40) Muller-Plathe, F.; van Gunsteren, W. F. *Polymer* **1997**, *38*, 2259–2268.
(41) Muller-Plathe, F. *J. Membr. Sci.* **1998**, *141*, 147–154.
(42) Chiessi, E.; Cavalieri, F.; Paradossi, G. *J. Phys. Chem. B* **2007**, *111*, 2820–2827.
(43) Longhi, G.; Lebon, F.; Abbate, S.; Fornili, S. L. *Chem. Phys. Lett.* **2004**, *386*, 123–127.
(44) Gangemi, F.; Longhi, G.; Abbate, S.; Lebon, F.; Cordone, R.; Ghilardi, G. P.; Fornili, S. L. *J. Phys. Chem. B* **2008**, *112*, 11896–11906.
(45) Brooks, B. R.; Brooks, C. L.; Mackerell, A. D.; Nilsson, L.; Petrella, R. J.; Roux, B.; Won, Y.; Archontis, G.; Bartels, C.; Boresch, S.; Caflisch, A.; Caves, L.; Cui, Q.; Dinner, A. R.; Feig, M.; Fischer, S.; Gao, J.; Hodoscek, M.; Im, W.; Kuczera, K.; Lazaridis, T.; Ma, J.; Ovchinnikov, V.; Paci, E.; Pastor, R. W.; Post, C. B.; Pu, J. Z.; Schaefer, M.; Tidor, B.; Venable, R. M.; Woodcock, H. L.; Wu, X.; Yang, W.; York, D. M.; Karplus, M. *J. Comput. Chem.* **2009**, *30*, 1545–1614.
(46) Berendsen, H. J. C.; Postma, J. P. M.; van Gunsteren, W. F.; Di Nola, A.; Haak, J. R. *J. Chem. Phys.* **1984**, *81*, 3684–3690.
(47) Lindahl, E.; Hess, B.; van der Spoel, D. *J. Mol. Mod.* **2001**, *7*, 306–317.
(48) van der Spoel, D.; Lindahl, E.; Hess, B.; Groenhof, G.; Mark, A. E.; Berendsen, H. J. C. *J. Comput. Chem.* **2005**, *26*, 1701–1718.
(49) Schuler, L. D.; van Gunsteren, W. F. *Mol. Simul.* **2000**, *25*, 301–319.
(50) Schuler, L. D.; Daura, X.; van Gunsteren, W. F. *J. Comput. Chem.* **2001**, *22*, 1205–1218.
(51) Lins, R. D.; Hünenberger, P. H. *J. Comput. Chem.* **2005**, *26*, 1400–1412.
(52) Berendsen, H. J. C.; Postma, J. P. M.; van Gunsteren, W. F.; Hermans, J. *Intermolecular Forces*; Reidel: Dordrecht, The Netherlands, 1981; 331−342.
(53) Hockney, R. W. *Methods Comput. Phys.* **1970**, *9*, 136–210.
(54) Ryckaert, J. P.; Ciccotti, G.; Berendsen, H. J. *J. Comput. Phys.* **1977**, *23*, 327–341.
(55) Luzar, A.; Chandler, D. *Nature* **1996**, *379*, 55–57.
(56) Luzar, A. *J. Chem. Phys.* **2000**, *113*, 10663–10675.
(57) Paul, S.; Chandra, A. *Chem. Phys. Lett.* **2004**, *386*, 218–224.
(58) Liu, P.; Harder, E.; Berne, B. J. *J. Phys. Chem. B* **2005**, *109*, 2949–2955.
(59) Allen, M. P.; Tildesley, D. J. *Computer Simulations of Liquids*; Oxford University Press: New York, 1987.
(60) Humphrey, W.; Dalke, A.; Schulten, K. *J. Mol. Graphics* **1996**, *14*, 33–38.
(61)

$$B = \frac{8}{3}\pi^2 \cdot RMSF^2$$

(62) (a) Singh, G. P.; Parak, F.; Hunklinger, S.; Dransfeld, K. *Phys. Rev. Lett.* **1981**, *47*, 685–688. (b) Koenig, S. H.; Hallenga, K.; Shporer, M. *Proc. Natl. Acad. Sci. U.S.A.* **1975**, *72*, 2667–2671. (c) Doster, W.; Bachleitner, A.; Dunau, R.; Hiebl, M.; Lüscher, E. *Biophys. J.* **1986**, *50*, 213–219. (d) Steinhoff, H. J.; Kramm, B.; Hess, G.; Owerdieck, C.; Redhardt, A. *Biophys. J.* **1993**, *65*, 1486–1495. (e) Denisov, V. P.; Halle, B. *Biochemistry* **1998**, *37*, 9595. (f) Teixeira, J. *Gen. Physiol. Biophys.* **2009**, *28*, 168–173.

(63) (a) Paradossi, G.; Cavalieri, F.; Chiessi, E.; Telling, M. T. F. *J. Phys. Chem. B* **2003**, *107*, 8363–8371. (b) Cavalieri, F.; Chiessi, E.; Finelli, I.; Natali, F.; Paradossi, G.; Telling, M. F. *Macromol. Biosci.* **2006**, *6*, 579–589.

(64) Tehei, M.; Franzetti, B.; Wood, K.; Gabel, F.; Fabiani, E.; Jasnin, M.; Zamponi, M.; Oesterhelt, D.; Zaccai, G.; Ginzburg, M.; Ginzburg, B. Z. *Proc. Natl. Acad. Sci. U.S.A.* **2007**, *104*, 766–771.

(65) (a) Netz, P. A.; Dorfmüller, T. *J. Phys. Chem. B* **1998**, *102*, 4875–4886. (b) Mijović, J.; Zhang, H. *J. Phys. Chem. B* **2004**, *108*, 2557–2563. (c) Chiessi, E.; Paradossi, G.; Cavalieri, F. *J. Phys. Chem. B* **2005**, *109*, 8091–8096.

(66) Bizzarri, A. R.; Cannistraro, S. *J. Phys. Chem. B* **2002**, *106*, 6617–6633.

(67) Matubayasi, N.; Levy, R. M. *J. Phys. Chem.* **1996**, *100*, 2681–2688.

(68) Pratt, L. R.; Pohorille, A. *Chem. Rev.* **2002**, *102*, 2671–2692.

(69) ten Wolde, P. R.; Sun, S. X.; Chandler, D. *Phys. Rev. E* **2001**, *65*, 011201–011209.

(70) (a) Yoshida, K.; Ibuki, K.; Ueno, M. *J. Chem. Phys.* **1998**, *108*, 1360–1367. (b) Haselmeier, R.; Holz, M.; Marbach, W.; Weingartner, H. *J. Phys. Chem.* **1995**, *99*, 2243–2246. (c) Shimizu, A.; Fumino, K.; Yukiyasu, K.; Taniguchi, Y. *J. Mol. Liq.* **2000**, *85*, 269–278. (d) Okouchi, S.; Moto, T.; Ishihara, Y.; Numajiri, H.; Uedaira, H. *J. Chem. Soc. Faraday Trans.* **1996**, *92*, 1853–1857. (e) Ishihara, Y.; Okouchi, S.; Uedaira, H. *J. Chem. Soc. Faraday Trans.* **1997**, *93*, 3337–3342. (f) Kaatze, U.; Gerke, H.; Pottel, R. *J. Phys. Chem.* **1986**, *90*, 5464–5466. (g) Wachter, W.; Buchner, R.; Hefter, G. *J. Phys. Chem. B* **2006**, *110*, 5147–5154. (h) Harris, K. R.; Newitt, P. J. *J. Phys. Chem. B* **1998**, *102*, 8874–8879.

(71) Chara, O.; McCarthya, A. N.; Ferrara, C. G.; Caffarena, E. R.; Grigera, J. R. *Physica A* **2009**, *388*, 4551–4559.

(72) Silvestrelli, P. L. *J. Phys. Chem. B* **2009**, *113*, 10728–10731.

(73) Paradossi, G.; Cavalieri, F.; Chiessi, E. *Carbohydr. Res.* **2005**, *340*, 921–927.

(74) Krynicki, K.; Green, C. D.; Sawyer, D. W. *Faraday Discuss. Chem. Soc.* **1978**, *66*, 199–208.

(75) Teixeira, J.; Bellissent-Funel, M. C.; Chen, S. H.; Dianoux, A. J. *Phys. Rev. A* **1985**, *31*, 1913–1917.

(76) Osaka, N.; Shibayama, M.; Kikuchi, T.; Yamamuro, O. *J. Phys. Chem. B* **2009**, *113*, 12870–12876.

(77) Singwi, K. S.; Sjolander, A. *Phys. Rev.* **1960**, *119*, 863–871.

(78) Ghugare, S. V.; Chiessi, E.; Telling, M. F.; Deriu, A.; Gerelli, Y.; Wuttke, J.; Paradossi, G. *J. Phys. Chem. B* Submitted for publication, 2010.

JP912209Z